Relation between Kinematic Boundaries, Stirring, and Barriers for the Antarctic Polar Vortex

BINSON JOSEPH* AND BERNARD LEGRAS

Laboratoire de Météorologie Dynamique, UMR8539, Paris, France

(Manuscript received 26 September 2000, in final form 17 July 2001)

ABSTRACT

Maximum stretching lines in the lower stratosphere around the Antarctic polar vortex are diagnosed using a method based on finite-size Lyapunov exponents. By analogy with the mathematical results known for simple dynamical systems, these curves are identified as stable and unstable manifolds of the underlying hyperbolic structure of the flow. For the first time, the exchange mechanism associated with lobe dynamics is characterized using atmospheric analyzed winds. The tangling manifolds form a stochastic layer around the vortex. It is found that fluid is not only expelled from this layer toward the surf zone but also is injected inward from the surf zone, through a process similar to the turnstile mechanism in lobe dynamics. The vortex edge, defined as the location of the maximum gradient in potential vorticity or tracer, is found to be the southward (poleward) envelope of this stochastic layer. Exchanges with the inside of the vortex are therefore largely decoupled from those, possibly intense, exchanges between the stochastic layer and the surf zone. It is stressed that using the kinematic boundary defined by the hyperbolic points and the manifolds as an operational definition of vortex boundary is not only unpractical but also leads to spurious estimates of exchanges. The authors anticipate that more accurate dynamical systems tools are needed to analyze stratospheric transport in terms of lobe dynamics.

1. Introduction

It is now well established that the springtime ozone depletion in the polar stratosphere depends on the ability of the polar vortex to preserve the polar air isolated from mixing with subtropical air (WMO 1999; McIntyre 1995). During winter, sharp gradients on potential vorticity (PV) and concentration of chemical compounds develop on the edge of the polar vortex as a result of diabatic descent and weak exchange between the vortex and the midlatitudes. This observation has led to the concept of a potential vorticity barrier (McIntyre and Palmer 1984; Holton et al. 1995) creating an almost insurmountable obstacle for the penetration of air from the outside while long and thin filaments of polar air are frequently ejected (Waugh et al. 1994; Plumb et al. 1994) and irreversibly stirred by Rossby waves in the *surf zone* (McIntyre and Palmer 1984; Juckes and McIntyre 1987) where they eventually mix with midlatitude air. Filaments can be seen as sloping sheets of PV or tracer, generated by the combined action of horizontal strain and vertical shear. It is also known that the southern (Antarctic) vortex is generally more stable, calm, persistent, and isolated than its counterpart in the Northern Hemisphere (Bowman 1993; Dahlberg and Bowman 1994). Hence, filamentation events in the Southern Hemisphere are also generally less intense than those from the northern vortex (Mariotti et al. 2000).

Over periods of less than about two weeks, diabatic motion is in general small in the lower stratosphere, so that the flow is well approximated as layerwise two-dimensional and incompressible on isentropic surfaces. Evidence suggests that chaotic advection is relevant to the stirring of stratospheric air (Pierrehumbert 1991a,b; Pierce and Fairlie 1993; Pierce et al. 1994; Waugh et al. 1994; Ngan and Shepherd 1999) down to horizontal scales of the order of 15–50 km where three-dimensional motion takes over (Balluch and Haynes 1997; Waugh et al. 1997) leading eventually to molecular mixing. It is also clear from the chaotic advection paradigm that the presence of many scales in the velocity field is not a prerequisite for complex deformation of material lines (Hénon 1966; Aref 1984; Ottino 1989).

Over the past two decades, the theory of dynamical chaos in Hamiltonian systems has found far reaching applications to chaotic transport and stirring in fluid mechanics (e.g., Ottino 1989; Zaslavsky 1998; Rom-

* Current affiliation: Department of Mathematics, Arizona State University, Tempe, Arizona.

Corresponding author address: Dr. Bernard Legras, Laboratoire de Météorologie Dynamique, 24 Rue Lhomond, 75231, Paris, Cedex 05, France.
E-mail: legras@lmd.ens.fr

Kedar et al. 1990).[1] Of central importance is the concept of local hyperbolicity and recurrence, which can be translated in common language by saying that stirring is produced by the repeated action of strain (stretching and folding) on tracer contours. In a stationary, two-dimensional (2D) flow, hyperbolic points are saddle-type stagnation points on the streamfunction map. Convergence of a flow toward a hyperbolic point, forward and backward in time, occurs along stable and unstable manifolds, respectively. The same property is also used to extend the definition of hyperbolic points to space–time *hyperbolic trajectories* in a time-dependent system (Coppel 1978; Malhotra and Wiggins 1999; Haller 2000; Haller and Yuan 2000). Such trajectories are material trajectories toward which other trajectories contained on two particular space–time surfaces are converging, respectively, forward and backward in time. The above noted surfaces in the time-extended phase space define the stable and the unstable manifolds of a time-dependent 2D flow.

Hyperbolic trajectories in 2D time-dependent flows quite often pass close to ''persistent'' instantaneous saddle points of the streamfunction map, but are different from them. Pairs of particles, initially straddling the stable manifold, separate apart along the two branches of the unstable manifold. This is also true for a stationary flow with a hyperbolic stagnation point. But the crucial difference is that, in the time-dependent flow, stable and unstable manifolds associated to one or several hyperbolic trajectories, typically, crosses and generates a complex tangle. Particle trajectories within such a tangle of manifolds are chaotic. Thus, stirring in the time-dependent flow can be very efficient through recurrent action of strain. A blob of fluid, released into such a chaotically stirring region, is first elongated and then turned into a complex folded structure as it is captured within the tangled manifolds. If the fluid can be assumed incompressible, the blob has to preserve its area while its perimeter increases exponentially, as do the length of any material curve. In the well-studied strictly periodic case, if the manifolds cross once, they must cross infinitely many times, each crossing being a past or future image of the first crossing at time instants that are integer multiples of the period of the Eulerian flow. Sophisticated perturbation methods can be applied if, in addition, the system is close to integrable. It is only recently that the quasiperiodic and the aperiodic situations (of the Eulerian flow) have been considered (Beigie et al. 1991, 1994; Malhotra and Wiggins 1999; Haller and Poje 1998; Haller 2000; Haller and Yuan 2000; Couliette and Wiggins 2000). In the aperiodic case, which is obviously more relevant from the perspective of transport and stirring in geophysical fluid dynamics, the manifolds may or may not cross or may only have a finite number of crossings and the hyperbolic trajectories may be of finite duration.

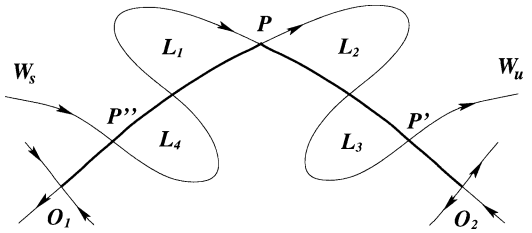

FIG. 1. Sketch of the hyperbolic structure and the turnstile mechanism exchanging lobes for a simple idealized flow with two hyperbolic points O_1 and O_2. The W_s and W_u are the stable and the unstable manifolds associated to O_1 and O_2, respectively.

When the flow is time periodic with period T, the stable/unstable manifolds form intersecting curves on an instantaneous flow map (or Poincaré map) at a constant phase of the flow, and one may consider lobes of fluid bounded by the segments of stable and unstable manifolds (see, e.g., Drazin 1992). In Fig. 1, lobe L_3 contains at time t the particles that were in lobe L_1 at time $t - T$ when the particles in P'' and P at time t were, respectively, in P and P'. Conversely lobe L_2 contains the particles that were in lobe L_4 at time $t - T$. Continuity implies that fluid on one side of the stable or instable manifold is mapped onto the same side. Because the Poincaré map is orientation preserving, the lobe will get mapped onto another lobe an even number of lobes ahead. Since the mapping is area preserving, the height of the lobe increases as it approaches the hyperbolic point because its base decreases (which follows from the fact that successive images or preimages of a point of intersection of stable and unstable manifolds get closer and closer as they approach the hyperbolic point). It is convenient to use the stable/unstable manifolds to define qualitatively different flow domains and to characterize exchanges between such domains. In particular, we can define a domain limited by the two thick lines in Fig. 1 joining the hyperbolic points to the crossing of the stable and the unstable manifold in P at a given time t. This is what we call a *kinematic boundary*. The mapping of the lobes L_1–L_4 described above generates a *turnstile* across the kinematic boundary with the fluid in lobes L_1 and L_4 changing side over a period T (Mackay et al. 1984; Rom-Kedar et al. 1990).

This approach is well suited to periodic or quasiperiodic flows and has been applied in several instances to simplified models of geophysical fluid dynamics (see, e.g., Duan and Wiggins 1996; del Castillo-Negrete 1998; Koh and Plumb 2000). However, one might face several difficulties when extending such ideas developed for periodic flows to aperiodic flows. A first difficulty is that the kinematic boundary is not materially preserved in time because one piece of manifold must be cut and another one pasted recurrently. The operation relies on the arbitrary choice of one of the many inter-

[1] We prefer here, after Eckart (1948), to use the word *stirring* instead of *mixing*, often used in the mathematical literature, to distinguish the irreversible molecular mixing from the reversible action of advection.

sections of the stable and unstable manifolds. For a periodic flow, where it is done once every period, it is usually easy to find on a given Poincaré map the intersection providing the least distorted boundary and to calculate the exchange by comparing this curve with itself one period later. For weakly perturbed periodic flow (so that no topological bifurcations is anticipated), it is possible to define and compute the areas of turnstile lobes, on a given Poincaré map, exchanging fluid from one side of the kinematic boundary to the other (Mackay et al. 1984; Rom-Kedar et al. 1990; Miller et al. 1997). This scheme seems unpractical for an aperiodic flow since the boundary has to be redefined at irregular intervals as the material line of the initial boundary gets deformed or because the whole hyperbolic structure changes along with the birth and death of hyperbolic trajectories, inducing numerous abrupt and spurious exchanges between the inside and the outside of the domain. Another difficulty, which is also present for periodic flows, is that owing to the complex tangle of intersecting manifolds, particles may go back and forth across the kinematic boundary. If this exchange is strong enough, steep tracer gradients, which are considered a main feature of the barrier effect in observations, need not develop along the kinematic boundary. We will see below that the high gradients rather tend to develop on the boundaries of the mixing region spanned by the tangle of manifolds. Indeed, some of the difficulties discussed above have been recognized by Koh and Plumb (2000), who made a previous attempt to apply the lobe dynamics approach to the mixing properties of the polar vortex.

Bowman (2000, manuscript submitted to *J. Atmos. Sci.*, hereafter BJAS) introduced a numerical method to detect stable and unstable manifolds of hyperbolic points as maximum stretching lines and applied it to the Southern Hemisphere stratosphere. He integrated, respectively, backward and forward in time the trajectories of particle pairs using interpolated analyzed winds and showed convincingly that a map of the unstable and the stable manifolds is obtained by plotting the initial location of particle pairs undergoing the largest separation. The rationale is that pairs straddling the stable manifolds separate along the two branches of the unstable manifold as they pass through the hyperbolic trajectory during a forward integration. Similar argument holds during a backward integration by exchanging the roles of the stable and the unstable manifolds. Applying this method to the springtime Antarctic polar vortex, BJAS points out long-lived hyperbolic structures on the vortex edge and the layering and tangling of stable and unstable manifolds around the vortex.

The major goal of this paper is to present some additional points to the study of BJAS. First, we present a closely related numerical method, based on finite-size Lyapunov exponents, for constructing hyperbolic manifolds, which like in BJAS are seen as maximum strechting lines. Our definition, however, differs from that of BJAS in a way on which depends the ability to detect the hyperbolic manifolds (see the appendix). By applying this method to the springtime Antarctic stratospheric flow, we demonstrate the clear connection between manifolds and filamentation events from the Antarctic vortex edge. We also show how the corotating Montgomery potential can be used to identify the approximate locations of hyperbolic trajectories and expected regions of filamentation. We show for the first time a clear instance where lobes and turnstile exchange can be characterized using observed winds. Finally, we discuss the relation between hyperbolic manifolds and the observed edge of the polar vortex.

In section 2, we describe the method used to diagnose the manifolds. Section 3 describes the data, and the results are presented in section 4. The notion of vortex edge is discussed in section 5, and section 6 offers further discussion and conclusion. The appendix provides a theoretical justification of the calculations.

2. Manifolds and the finite-size Lyapunov exponents

The infinitesimal Lagrangian dispersion of tracers is characterized by the Lyapunov exponent

$$\lambda(\mathbf{x}, t) = \lim_{T\to\infty} \lim_{\delta(\mathbf{x},t,0)\to 0} \frac{1}{T} \ln\frac{\delta(\mathbf{x}, t, T)}{\delta(\mathbf{x}, t, 0)}, \qquad (2.1)$$

where $\delta(\mathbf{x}, t, T)$ is the separation at time $t + T$ of a particle pair initially centered in $\mathbf{x}$ at time t. Under the incompressibility assumption, $\lambda(\mathbf{x}, t)$ is also the growth rate of tracer gradient perpendicularly to the direction of separation (Batchelor 1952). In practice, the Lyapunov exponent is uniform over any domain that is well mixed in the long time limit. This does not make it a very useful measure for space and time-dependent dispersion properties.

The finite-time Lyapunov exponent (FTLE), is defined for finite T by removing the first limit in the right-hand side of (2.1) and taking T of the order of the integral scale of the flow. The usefulness of this quantity in identifying qualitatively different mixing regions in atmospheric flows has been demonstrated in several studies (Pierrehumbert 1991a; Pierrehumbert and Yang 1993; Pierce and Fairlie 1993; Pierce et al. 1994). The pair separation method introduced by BJAS approximates the FTLE when the separating particles stay very close but differs for finite separation. We show in the appendix that pairs straddling the hyperbolic manifolds separate to a finite distance of order the characteristic scale of the flow faster than all other pairs in their vicinity. It has, however, been pointed out by Haller (2000), and this is demonstrated in the appendix, that the distribution of pair separation is typically a ''fuzzy'' view of the hyperbolic manifolds. Here, we use a closely related technique, based on finite-size Lyapunov exponent (FSLE), which results in a less fuzzy distribution and allows the manifold structures to emerge, more nat-

urally, as the threshold rate of separation is increased. FSLE was introduced in the context of predictability in systems with many characteristic scales by Aurell et al. (1997) and has been used to study tracer dispersion in enclosed flow domain (Artale et al. 1997) and buoy dispersion in semienclosed oceanic basins (Lacorata et al. 2001).

For a given finite initial separation $\delta(\mathbf{x}, t, 0) = \delta_0$ and a growth factor r, the FSLE is

$$\mu(\mathbf{x}, t, \delta_0, r) = \frac{1}{\tau} \ln r, \tag{2.2}$$

where τ is such that $\delta(\mathbf{x}, t, \tau) = r\delta_0$. Hence τ is the required time to increase the separation by a factor r. When r is of the order of a few units, μ describes the diffusion properties at scale δ_0 (Artale et al. 1997; Boffetta et al. 2000), which may differ from that at infinitesimal scale if the flow is turbulent, in agreement with Richardson's theory (Richardson 1926) of relative dispersion. When $r \gg 1$, the stable and unstable manifolds are obtained by plotting the extrema of μ for, respectively, forward and backward interation in time (see the appendix). Here the resolution δ_0 is limited by the need to grow the separation to synoptic scale within a duration τ of the order of the integral scale.

Although the atmospheric flow is much more complicated than the examples used in the appendix, we assume here that the FSLE method is able to detect the hyperbolic manifolds of the flow given by the atmospheric dataset described below.

Our implementation of the FSLE method is as follows. First, we initialize a quasi-uniform distribution of particles in the flow domain, which is the 500-K isentropic surface covering the entire Southern Hemisphere. Considering $N = 180$ equally spaced parallels from equator to pole, we put $4N \cos\phi$ regularly spaced points on each circle of latitude ϕ, resulting in $M = 82\,779$ particles to cover the hemisphere with a resolution of 55 km. Then, we consider a slightly perturbed distribution of points about the original reference distribution that generates a set of M pairs with the reference distribution. We choose the perturbation δ_0, for convenience, to be 11 km (0.1°) in the meridional direction. Then, we calculate the evolution of the two distributions forward and backward in time, and we check the times τ_{ij} at which the jth pair separation, measured in great circle distance, first crosses predefined threshold distances given by $\delta_i = r_i\delta_0$ where r_i is chosen among {5, 10, 20, 50, 75, 100} in our case. Then, we use (2.2) to define the FSLE $\mu(\mathbf{x}_j, t, \delta_0, r_i) = \log r_i/\tau_{ij}$. If a threshold distance is not reached by the particle in the finite time of consideration (typically 9 days in our calculations), FSLE values are zeroed out for such least stretching points and this threshold. Finally, we map the FSLE values on to the initial locations $\{\mathbf{x}_j\}$ of particles in the reference distribution. At moderately high threshold distances (which is typically 50–100 times the initial separation in this study), we see the emerging structures of hyperbolic manifolds identified as the maximum stretching lines.

3. Data and numerical integration

All the calculations included in this study are done using the wind fields from the spectral T106 meteorological analyses of the European Centre for Medium-Range Weather Forecasts (ECMWF) on 15 pressure levels. This is a main novelty of this work to use real atmospheric data. The required isentropic trajectory and contour advection calculations are done with modified versions of the code used in Mariotti et al. (1997). The available 6-h T106 spectral coefficients of ECMWF winds are interpolated in time, using cubic splines, to 15-min intervals. The wind is vertically interpolated from pressure to isentropic levels on the Gaussian collocation grid using a combination of interpolation methods (Akima 1991; McAllister and Roulier 1981) in order to prevent spurious oscillations and is then calculated on a regular 162 × 256 latitude–longitude spherical grid. It is further interpolated at the location of the particle by a bilinear interpolation within the mesh of the four adjacent points on the grid. Advection of particles is done in the 3D Cartesian coordinates, followed by a projection back to the sphere, using a fourth-order Runge–Kutta time scheme with a 30-min time step.

4. Results

a. Manifolds

Figure 2 shows, for 25 October 1996 in the Southern Hemisphere, the stable and unstable manifolds constructed by the FSLE method, superimposed on the PV map for the same day.[2] The hyperbolic manifolds are localized by pairs that have reached the separation $r = 75$ within less than 9 days. Other points are blanked out. The alignment of the dots suggests, by analogy with the examples of the appendix, that our algorithm provides a good approximation of the hyperbolic manifolds. Both the stable and the unstable manifold exhibit filamentary structures surrounding the vortex and extending arms within the surf zone. The PV filament that is ejected from the vortex southwest of Australia follows one branch of the unstable manifold. On the contrary, no structure is visible within the PV field in the surf zone that is associated with the stable manifold. The manifolds do not self-intersect, as implied by the uniqueness of solution curves, but the stable and the unstable manifolds are crossing several times. In particular, they cross at O_1 where the PV filament is emitted, indicating, according to the terminology of dynamical systems theory (cf. Haller and Poje 1998; Haller and Yuan 2000), the presence of a hyperbolic trajectory.

[2] Other sequences of October 1996 are presented in BJAS.

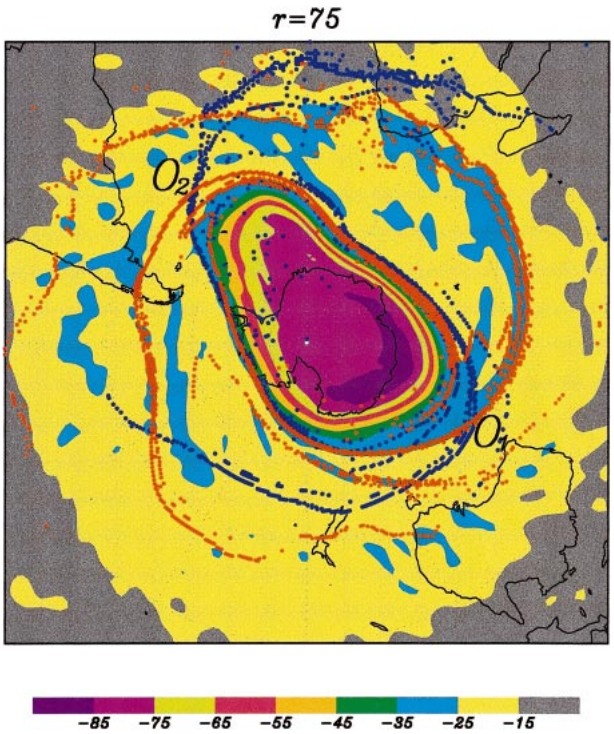

FIG. 2. Contours: potential vorticity map at 1200 UTC 25 Oct 1996 and on the isentropic level $\theta = 500$ K from the T106/L15 spectral analysis of ECMWF. Color scale is in PV units (PVUs) (1 PVU = 10^{-6} K kg^{-1} m^2 s^{-1}). Dots: initial locations of pairs that have grown their separation by a factor $r = 75$ within 9 days; red: backward integration (unstable manifold); blue: forward integration (stable manifold).

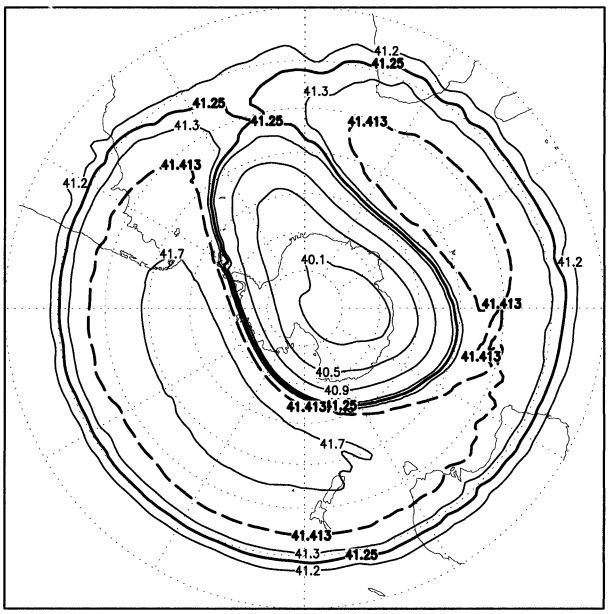

FIG. 3. Montgomery potential for the same time and the same level as Fig. 2 after removing a solid body of angular velocity $\Omega = 5 \times 10^{-6}$ s^{-1} around the polar axis. Units are in 10^4 m^2 s^{-2}.

Several intersections also occur in the South Atlantic east of Patagonia where the absence of PV filament does not allow us to formally identify which one is a hyperbolic trajectory. We know, however, from the topology of the flow and the manifolds, that the most likely location of the hyperbolic trajectory in this map is O_2, as will be confirmed shortly.

The branches of stable and unstable manifolds lying between O_1 and O_2 and connecting these two points delineate a fairly well-defined kinematic boundary. It is, however, visible that the vortex edge defined by the maximum PV gradient lies inside this boundary. For the moment, we denote as the *collar* the region enclosed between these two boundaries. See section 5 below.

We also applied Bowman's method to the same data and found a good agreement with our results. It appears that the saturation effects (see example II in the appendix) are not important over 1 to 2 weeks for the polar vortex.

b. Stagnation points

Since stratospheric flow is largely nondivergent, the saddles of the streamfunction map are instantaneous stagnation points of the flow. Under the quasigeostrophic approximation, the streamfunction on isentropic surfaces is the Montgomery potential $M = c_pT + gz$. In order to account for the rotation of the vortex, a solid body rotation with angular velocity ω is removed from M. From the visual inspection of vortex rotation during October 1996, we choose $\omega = 5 \times 10^{-6}$ s^{-1}, corresponding to a period of 14.5 days. Figure 3 shows the contours of $M - \frac{1}{2}R^2\Omega\omega \cos 2\varphi$, where Ω is the earth's angular velocity, R is its radius, and φ is the latitude, for the same time and level as Fig. 2. The saddles in this map can be followed by continuity over (at least) 3 weeks surrounding 25 October 1996 although they are moving slowly in the rotating frame. It is natural to expect that persistent stagnation points indicate the presence of hyperbolic trajectories but the hyperbolic trajectories do not generally coincide with sequences of stagnation points. While hyperbolic trajectories are independent of the frame, the stagnation points depend on the value of ω and there is no simple way to define the appropriate moving frame at a given time, which indeed may vary from one stagnation point to another. It is only when the flow pattern is weakly unsteady, as it is the case here in the rotating frame, that the saddle points and the hyperbolic trajectories are in close proximity (see also Haller and Poje 1998).

c. Turnstile

Figure 4 shows an enlargement of the manifold structure in Fig. 2 near the location of the hyperbolic trajectory O_2. A smaller value of r has been used here to gather more points but this at the cost of a fuzzier appearance of some branches. We have also halved δ_0 to

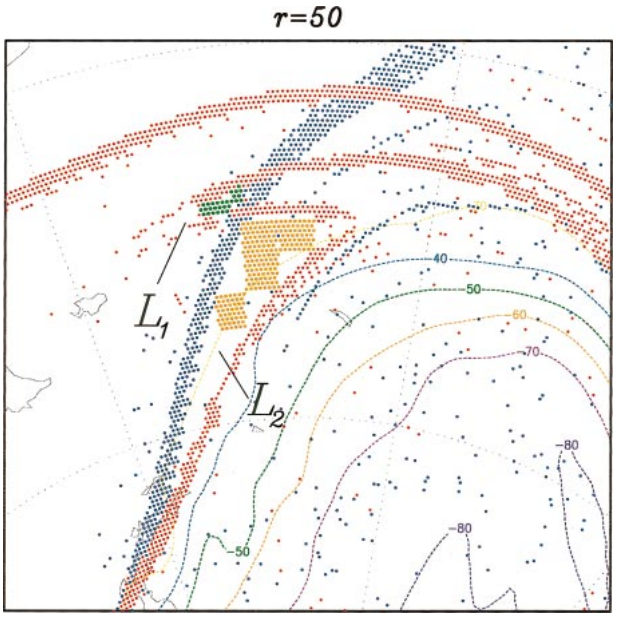

FIG. 4. Enlargement of the manifold structure near the hyperbolic point O_2 in Fig. 2 for $r = 50$. In green and orange, locations of the blobs of points used to sample the two lobes L_1 and L_2 formed by the crossing of the stable and the unstable manifold near O_2.

0.05° and doubled N to 360. We see that the hyperbolic manifolds intersect in a complex way generating a tangle of lobes. In particular, two well-defined lobes L_1 and L_2 are identified west of the hyperbolic point. Lobe L_1 lies within the collar while L_2 lies outside. Other more elongated lobes are visible along the branch covering the south of Latin America. We know from dynamical systems theory (see, e.g., Mackay et al. 1984; Rom-Kedar et al. 1990, for a discussion) that this structure should be associated with an exchange mechanism. In order to check this property, a set of trajectories have been calculated backward and forward in time for the initial conditions shown in Fig. 4 within the two adjacent lobes L_1 and L_2.

Figure 5 shows the result of the forward integration. The orange points are dispersed along the edge of the vortex while the green points move away, being fully separated by more than 2000 km from the vortex within 2 days, along the unstable manifold associated to O_2. Figure 6 shows the results of the backward integration where it appears that the green points are coming from the edge of the vortex while the orange points were all at distance 7 days before 25 October along the stable manifold of O_1. To our knowledge, this is the first time that this *turnstile* effect based on lobe dynamics has been demonstrated using atmospheric analyzed winds.[3] Notice that the separation of the two clouds of points does not occur near the same hyperbolic trajectory in the forward and in the backward direction. This is an effect of the heteroclinic connection between the two hyperbolic trajectories, which illustrates also that the exchange process is highly nonlocal. On 3 November, part of the orange set is being expelled within a filament. Its residence time within the collar has not exceeded 10 days.

Henceforth we see that the ejection of filamentary structure is not one way but is accompanied by the injection of midlatitude air that gets incorporated within the collar. By estimating the area of the two lobes delineated in Fig. 4 we could in principle estimate the ratio of the injected fluid to the ejecta. This cannot be done accurately here owing to the lack of resolution of the unstable manifold bounding L_2 but, since lobe L_1 appears larger than lobe L_2, there is more fluid entering the collar than in the ejecta. If the flow was periodic, the two should be equal but there is not such a constraint for aperiodic flows. We do not know, however, from our purely Lagrangian analysis whether the injected air will get mixed within the collar air or will be part of a new ejecta before being totally mixed, as on 3 November 1996. As time proceeds with new events, the collar of the vortex will contain a sandwich of air of different origin, which is often reported from airborne sections (Tuck 1989).

5. The vortex edge

It has already been mentioned in the introduction that using pieces of stable and unstable manifolds to define vortex boundary is inconsistent for aperiodic flows. We see here that the complexity of the exchanges with air moving rapidly in and out the collar hardly matches with the one way flux from the vortex to the outside which is one condition of the observed isolation of the vortex (Koh and Plumb 2000). In fact, the question is to properly define the vortex edge.

A practical definition of the edge is the location of the highest gradient in PV or in chemical compounds. In a simple model using a PV patch and contour dynamics with surgery on the sphere, Koh and Plumb (2000) show that the vortex edge which is a single vorticity contour does not coincide with the manifolds and state that ''there are certain parameter range in which a few events occur in which material is stripped off the vortex, following which transport across the edge ceases, even though turnstile transport continues indefinitely within the critical layer.''

In the stratosphere, the vortex cannot be prescribed but has to be maintained as a balance between diabatic and kinematic processes. Since the vortex is not circular, the location of the edge is best plotted in terms of equivalent latitude ϕ_e that is defined from the area A of a given PV contour as $A = 2\pi R^2(1 - \sin\phi_e)$. We see (in Fig. 8) that the PV gradient is sharply peaked near $\phi_e = 65°$S when we use the PV calculated from the T106 analysis. Using instead a reconstructed PV obtained by

[3] One application using oceanographic data has been done by Coulliette and Wiggins (2000).

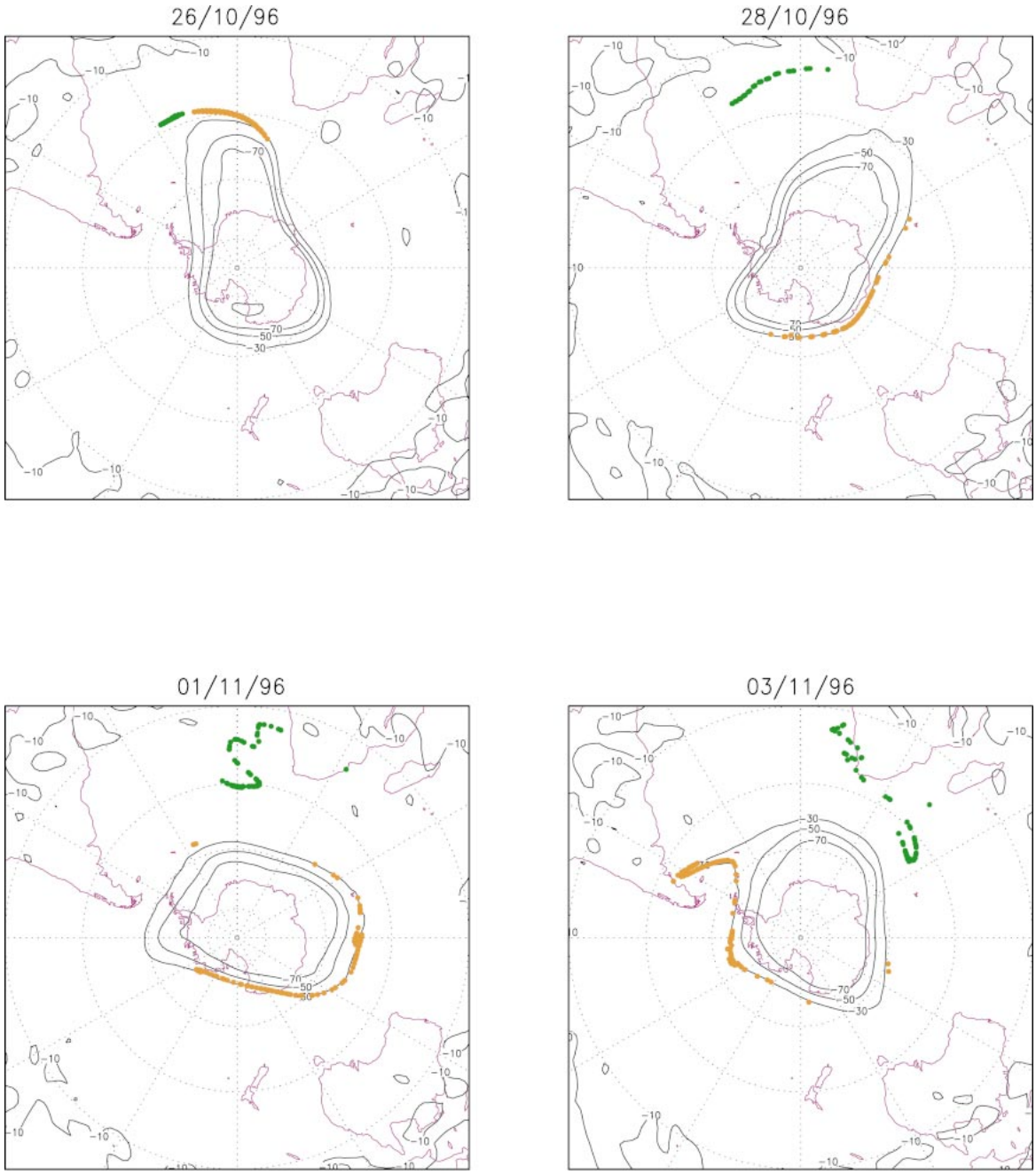

FIG. 5. Forward temporal evolution of the blobs contained within the two lobes defined in Fig. 4 at 1200 UTC 26, 28 Oct and 1, 3 Nov 1996. Solid lines are PV contours.

contour advection over 8 days (not shown) provides essentially the same result. This indicates that the maximum gradient also tends to follow a PV contour that is close to a material line as long as the diabatic effects are neglected.

Setting the edge as the location of the maximum gradient is a purely diagnostic definition calling for a dynamical explanation of gradient generation and maintenance. The *effective diffusivity* has been introduced (Nakamura 1996; Haynes and Shuckburgh 2000) for the consideration of the evolution of a conservative tracer $c(\mathbf{x}, t)$ governed by two-dimensional advection–diffusion. For each value C of the concentration, the function $A(C, t)$ is defined as the area of the region for which the tracer concentration $c(\mathbf{x}, t)$ is greater than or equal to C. By definition $A(C, t)$ is a monotonic function of C and can be inverted as $C(A, t)$. Nakamura (1996) showed that the function $C(A, t)$ satisfies the equation

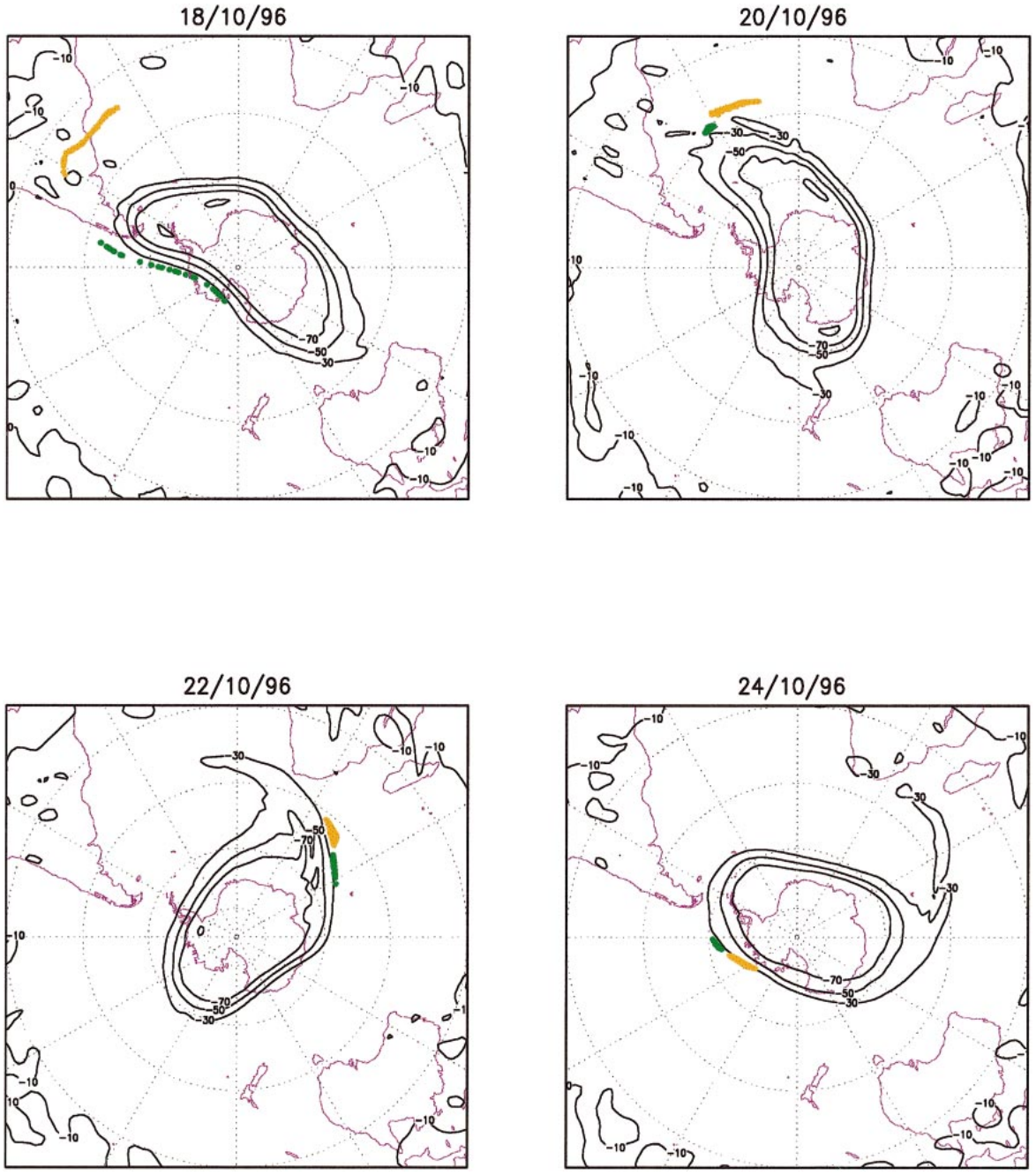

FIG. 6. Same as Fig. 5 but for backward integration and at 1200 UTC 18, 20, 22, and 24 Oct 1996.

$$\frac{\partial C(A, t)}{\partial t} = \frac{\partial}{\partial A}\left[\kappa L_e \frac{C(A, t)}{\partial A}\right], \tag{5.1}$$

where the equivalent length of the contour C is defined by

$$L_e^2(A, t) = \left(\frac{\partial C}{\partial A}\right)^{-2} \frac{\partial}{\partial A} A(|\nabla c|^2), \tag{5.2}$$

in which A denotes the integral of a scalar over the area bounded by the contour C.

The effective length is estimated from a contour advection of PV over a duration of 10 days ending on 27 October 1996 (cf. Mariotti et al. 1997). As contour advection generates endless increasing contour length, we apply contour surgery (Dritschel 1989) with surgery scale $d = 20$ km. It can be demonstrated for advection diffusion equation that contour length is a lower bound

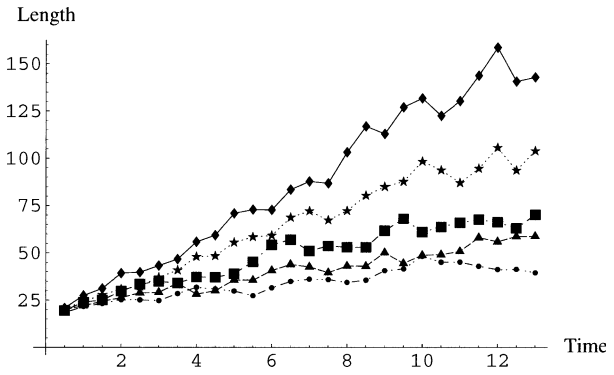

FIG. 7. Contour length growth for contour advection with surgery and a contour corresponding to −25 PVU located within the surf zone. The curves are ordered from top to bottom in increasing order of the surgery scale. Values of the surgery scale are $d = \{5, 10, 20, 30, 40\}$ km. The contour length is normalized by the length of the latitude circle for the corresponding equivalent latitude.

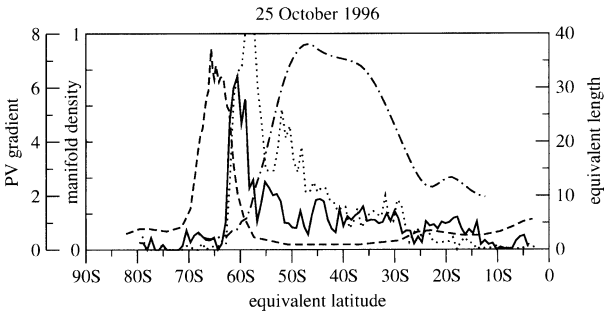

FIG. 8. Dash: PV gradient; unit: PVU per degree. Mixed: equivalent length normalized by the length of the latitude circle for the corresponding equivalent latitude. Solid: density of the stable manifold calculated as the number of points shown in Fig. 2 falling within latitude bands of width 0.09° in equivalent latitude; unit: number of points per surface area of the sphere with radius unity, divided per 2000. Dotted: same for the unstable manifold.

of the effective length (Haynes and Shuckburgh 2000) but it has been shown that in practice the two quantities stay always very close (E. Shuckburgh 2001, personal communication). Although contour surgery is not exactly a diffusive process, we use the contour lengths from our calculations as estimates of the effective lengths with a diffusive scale equal to 20 km. Figure 7 shows that the contour length saturates in about 10 days for this value of d and a contour within the surf zone. Figure 8 shows the smoothed equivalent length averaged over five adjacent days (23rd to 27th) centered on 25 October. The maximum at 50°S is associated to the efficient cross-latitude stirring within the surf zone. The minimum coincides with the maximum PV gradient. Its very low value corresponds to a contour length less than two times that of the equivalent latitude circle, indicating the stability of material trajectories on the edge of the vortex.

In order to relate these diagnostics to the kinematic structure of the flow, Fig. 9 shows the distribution of points retained on the manifolds in Fig. 2 as a function of the equivalent latitude, and Fig. 8 shows the manifold density, that is the normalized number of points falling within a latitude bin.[4] This is a measure of space filling by the resolved manifolds or, in other words, of the stirring efficiency within a latitude band. It is striking that, for both the stable and the unstable manifolds, density maxima are observed within a layer of approximately 10° in latitude between 55° and 65°S, north of the vortex edge. We call this layer, which embeds the previously defined collar, the *stochastic layer* because the density of the manifolds and their numerous intersections indicates strong stirring, and probably mixing, with midlatitude air. The distribution tail in Fig. 8, extending toward midlatitude, is tracing the dilution of the manifolds as the distance is increasing from the stochastic layer.

We now see clearly the relation between the hyperbolic manifold structure and the vortex edge. The hyperbolic points and the manifolds are embedded within the stochastic layer outside the vortex edge. This latter is nothing but the southward closure of the stochastic layer. For a periodic two-dimensional flow such boundaries exist as invariant KAM tori and are perfect barriers for nondiffusive motion. In this case, an initially smooth tracer gradient across this barrier is soon transformed into a steep profile because stirring brings fluid with very different tracer concentration on the stochastic side of the barrier assuming that the stochastic layer spans a wide enough range in the space of tracer concentration. Though this mechanism has not yet been generalized to aperiodic flows in the literature, our results clearly suggest that it is relevant to the maintenance of the polar vortex edge.

In order to demonstrate that this property is not observed by chance at a given date, we show in Fig. 10 the same analysis performed at two other dates, which entirely corroborates our findings.

6. Discussion

We have applied a technique based on FSLE to identify hyperbolic manifolds in the Antarctic lower stratosphere. Hyperbolic manifolds found in this study roughly follow the instantaneous heteroclinic connections deducible from a dominant wavenumber 2 pattern in the corotating streamfunction. The stable and unstable manifolds span a stochastic layer just outside of the vortex edge and extend far outside the vortex within the surf zone. The lobes generated by intersecting hyperbolic

[4] In purely periodic flows, the manifolds are dense objects but may exhibit apparent anomalous scaling over a finite time interval (as numerically shown by Benettin et al. 1986) and our counting would scale with the sampling resolution. In aperiodic flows and for finite-time hyperbolic structure, the manifolds are defined up to some uncertainty due to incomplete convergence and thus can be considered as thick structures (Haller 2000; Haller and Yuan 2000). A more elaborate discussion on this matter is beyond the scope of this study.

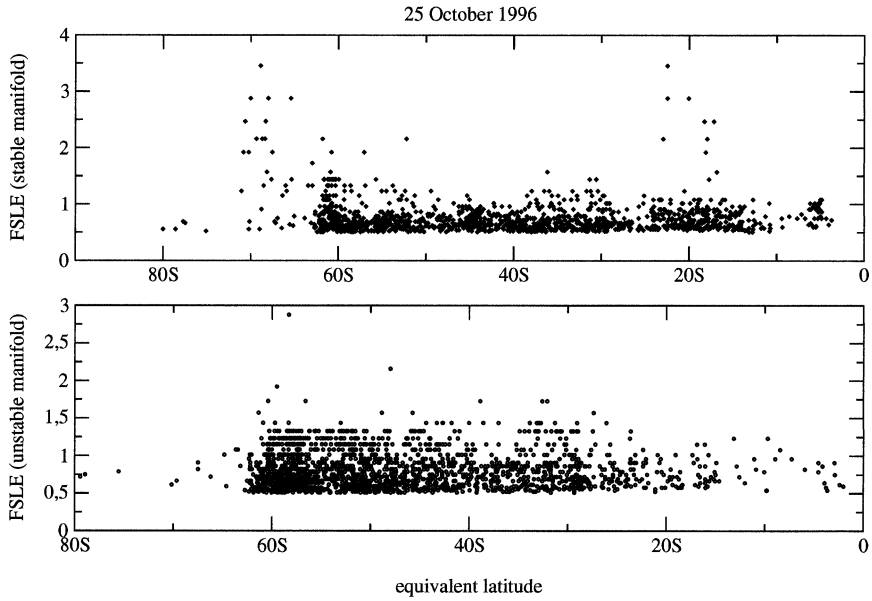

FIG. 9. Distribution of points belonging to the manifolds in Fig. 2 and value of the FSLE as a function of equivalent latitude. The threshold is due to the selection of pairs separating by $r = 75$ in 9 days or less. Unit: day^{-1}.

manifolds appear to govern the exchange between the stochastic layer and the surf zone in good agreement with dynamical systems theory.

We have shown, however, that the instantaneous kinematic boundary formed by pieces of hyperbolic manifolds surrounding the vortex does not match the contour of maximum PV gradient around the vortex across which exchanges reach a minimum. Identifying the kinematic boundary as the vortex boundary leads to diagnose spurious exchanges between the vortex and the outside as already found by Koh and Plumb (2000).

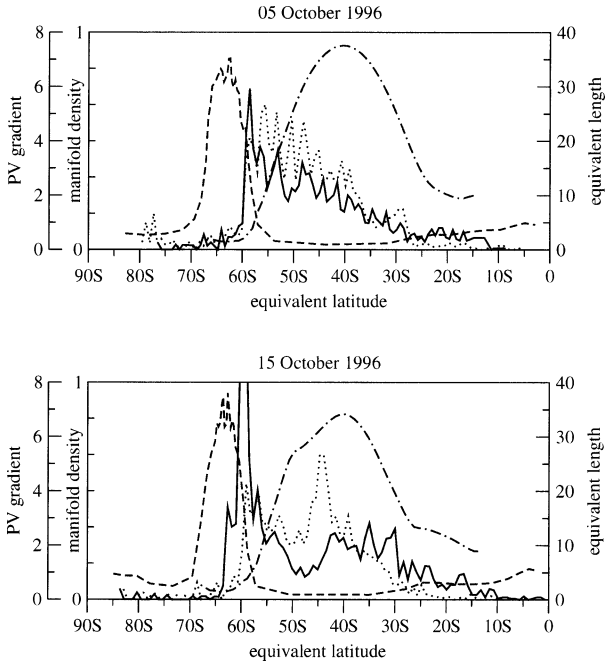

FIG. 10. Same as Fig. 8, but for 5 and 15 Oct 1996.

The vortex edge appears, in fact, as the interior closure of the stochastic layer. Consequently, the exchanges between the vortex and the exterior are not related with the turnstile effect of lobe dynamics. Under the idealized approximation of a periodic flow and vanishing diffusion, they may vanish while lobe dynamics still continues to transfer fluid parcels back and forth between the stochastic layer and the surf zone. Under aperiodic motion, the tangle of intersecting manifolds is evolving and changing structure with time as hyperbolic points and associated manifolds appear and disappear. Therefore, the stochastic layer and its interior closure need to be defined over time intervals whose length is such that isentropic advection dominates over diffusion and diabatic processes. From one interval to the next, the new stable manifolds may penetrate inside the previously isolated vortex, stripping away some poaches of vortex air that are incorporated into the stochastic layer. It is also possible that the new closure lies outside the old one, resulting in intrusion of subtropical air inside the vortex where it is eventually mixed by the horizontal shear and diffusion (Rhines and Young 1983). Many minor events of this type may produce significant exchanges between the vortex and the stochastic layer and by induction between the vortex and the surf zone. Notice that this dynamic was partly uncovered by Sobel and Plumb (1999), who diagnosed an entrainment layer surrounding the vortex.

It was recently shown (Plumb et al. 2000) that mixing across the vortex edge is able to produce separate com-

pact tracer relations within the vortex that cannot be attributed to chemistry. The effect is enhanced if mixing occur between several reservoirs. This is the case if the turnstile effect is able to bring air from a broad range of latitudes into contact with the vortex edge.

Contour advection or reverse domain filling techniques do provide a high-resolution instantaneous picture of the deformed nature of contours at any given instant. But it is not an easy task, by piecing together many such pictures, to deduce the (Lagrangian) transport characteristics or boundaries causing exchanges from one subdomain to another. In contrast, manifold structures do contain Lagrangian information, and they allow one to say where do the lobes come from or where do they go.

Our result and discussion relies on the presence of persistent hyperbolic trajectories near the edge of the polar vortex. In the examples shown here, this is due to a stable wavenumber 2 pattern that dominates over most of October 1996. The mathematical definition of hyperbolic trajectories for aperiodic flows (Malhotra and Wiggins 1999; Haller and Poje 1998; Haller 2000) is based on the local convergence of trajectories for backward and forward integrations and the stable and unstable manifolds can be constructed as the nonlocal extension of the local eigenspaces. Hyperbolic trajectories defined over a finite time T are not unique, they all lie within a tube in the space–time domain with a diameter of order $\exp(-sT)$ where s is the average magnitude of the strain (Haller 2000). The length of the manifolds is also finite, of order UT where U is the average magnitude of the velocity. Therefore, it is only when the hyperbolic trajectories survive for durations of the order of the integral time of the flow that the hyperbolic manifold structure may develop and span a sufficiently wide domain for lobe dynamics to be relevant. In this case the manifolds fill a layer just outside the vortex edge where they form a complex tangle which can be treated as a stochastic layer while their structure within the much wider surf zone remains essentially untangled and should be treated as long-range ballistic transport.

On the contrary, when hyperbolic trajectories are of short duration compared to the integral scale, the associated domain spanned by the manifolds is small, and stirring processes are local in space and time. As a limit one should recover the random strain Kraichnan's model where the velocity is uncorrelated in time. It is worth noticing that it has been recently shown (Kraichnan 1994; Chen and Kraichnan 1998; Frisch et al. 1998) that advection of passive scalars by random flows generically produces large plateaus of passive scalar concentration separated by sharp transitions as soon as the velocity contains many scales of motion.

Commonly, natural flows fall between two extrema, the periodic flow on one side and the fully random flow on the other side, for which theoretical results are well established. Accurate diagnostics of the distribution of hyperbolic trajectories and of their duration is required to better understand the dynamical processes of mixing. The FSLE method is probably only a first step and a simple diagnostic tool that should be supplemented by more sophisticated approaches such as that described in Malhotra and Wiggins (1999), Haller (2000), Haller and Yuan (2000), or Haller (2001).

Acknowledgments. The first author acknowledges the support of EU Grant ENV4-CT97-0546. We thank G. Haller for useful comments and E. Shuckburgh for numerous corrections.

APPENDIX

Identification of Hyperbolic Invariant Manifolds by FSLE

The fundamental concept behind the separation methods, Bowman's and ours, is that pairs of particles straddling the stable manifold of a hyperbolic trajectory separate faster than other pairs in their vicinity under forward temporal evolution. Hence, the stable manifold is visualized as the local maxima of the pair separation or of the FSLE. The unstable manifold is obtained in the same way by backward temporal integration.

Near a simple stagnation point of a stationary two-dimensional flow, the velocity field is locally described by ($u = \gamma x$, $v = -\gamma y$) with $\gamma > 0$. Within the region where this approximation is valid, all pairs separate in the x direction at the same exponential rate γ without regard to their initial location. All trajectories have the same stability properties for this simple linear flow and this is correctly highlighted by the separation methods. This is still true for the trajectories of any linear system (homogeneous or inhomogeneous). This teaches us that nonlinearity is essential to distinguish hyperbolic trajectories as unique among other trajectories.

As we shall see in the following examples, it is apparent that the two methods work because the exponential separation of pair trajectories is localized near the hyperbolic trajectories while pairs separate much slowly, generally linearly with time, in other regions. For nonintegrable systems, separation is not only directly associated with the hyperbolic trajectory but with all intersections of the stable and unstable manifolds. We believe that these properties are common to most bounded or periodic incompressible flows.

It is, however, clear that maximum separation lines may sometimes generate artifacts. A simple parallel flow with a strong shear maximum at some point of its section generates there a line of maximum stretching. Over a short enough time interval and with limited resolution data it may not be possible to distinguish strong linear growth from an exponential growth.

a. Example I: Locally hyperbolic flow

We first consider the stationary flow described by the streamfunction $\psi(x, y) = -\tanh x \tanh y$, which is locally

hyperbolic near the origin and reduces to a pure shear flow at distance. The y axis and the x axis are trivially the stable and the unstable manifolds of the hyperbolic fixed point at the origin.

For one point initially located at (x_0, y_0) the required time to reach abscissa x is

$$t = \frac{1}{2(1+\psi^2)} \log\left[\frac{-1+\psi^2+(1+\psi^2)\cosh 2x}{-1+\psi^2+(1+\psi^2)\cosh 2x_0}\right], \tag{A.1}$$

which can be written as

$$\cosh 2x = w \cosh 2x_0 - (w-1)\frac{1-\psi^2}{1+\psi^2}, \tag{A.2}$$

with $w = \exp[2t(1+\psi^2)]$.

We assume that all trajectories start from a given $y = y_0$. Hence we need only to consider the dispersion in the x direction. We also assume that trajectories are in the vicinity of the hyperbolic invariant manifolds, that is $\psi = -x_0 \tanh y_0$ is a small parameter. If we further assume that the final position x is such that $e^x \gg e^{-x}$, (A.2) reduces to

$$|x| = t(1 + x_0^2 \tanh^2 y_0) + \log|x_0| - \log \cosh y_0. \tag{A.3}$$

For a pair initially located at $\{x_0 + \frac{1}{2}\delta x_0, x_0 - \frac{1}{2}\delta x_0\}$, with both points on the same side of the y axis, the separation at time t under the above assumptions is

$$\delta x = 2t|x_0|\delta x_0 \tanh^2 y_0 + \log\left(\frac{x_0 + \frac{1}{2}\delta x_0}{x_0 - \frac{1}{2}\delta x_0}\right). \tag{A.4}$$

If $x_0 \gg \delta x_0/2$, the second term on the right-hand side can be neglected and we have

$$\delta x = 2t|x_0|\delta x_0 \tanh^2 y_0. \tag{A.5}$$

If now the pair straddles the y axis and t is large enough to satisfy (A.3) for both elements of the pair, the separation at time t is

$$\delta z = 2t + 2t\left(x_0^2 + \frac{1}{4}\delta x_0^2\right)\tanh^2 y_0 + \log\left(\frac{1}{4}\delta x_0^2 - x_0^2\right) - 2\log\cosh y_0, \tag{A.6}$$

which is approximated by

$$\delta x = 2t + \log\left(\frac{1}{4}\delta x_0^2 - x_0^2\right). \tag{A.7}$$

This separation is maximum at $x_0 = 0$. The ratio with that given in (A.5) is $(|x_0|\delta x_0 \tanh^2 y_0)^{-1}$.

This is illustrated in Fig. A1, which shows the pair separation and the FSLE for the same set of parameters.

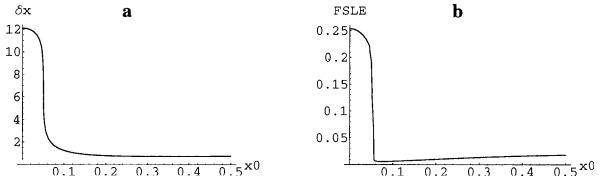

FIG. A1. (a) Pair separation at time $t = 8$ as a function of x_0 for $y_0 = 2$ and $\delta_0 = 0.1$. (b) FSLE as a function of x_0 for $y_0 = 2$, $\delta x_0 = 0.1$ and a final separation $\delta x = 4$.

Both methods provide a clear identification of the stable manifold within a spatial resolution equal to the pair distance. A sharp drop of the pair separation and the FSLE occurs near $x = \pm\delta_0/2$ as one element of the pair crosses the y axis.

b. Example II: The pendulum flow

We now consider the case of the stationary flow described by $\psi = \frac{1}{2}y^2 - \cos x$, which is equivalent to the standard pendulum problem. This is a kinematic model of a shear layer with an elliptic fixed point at the origin and hyperbolic points in $y = 0$ and $x = \pm\pi$. We assume that the domain is periodic in x with period 2π. Trajectories with $-1 < \psi < 1$ are rotating around the elliptic fixed point while trajectories with $\psi > 1$ move always in the same direction. The separatrix between these two families of trajectories connects the hyperbolic points for $\psi = 1$.

This problem is integrable in terms of elliptic functions and elliptic integrals (Lawden 1989). All trajectories except those on the separatrix are periodic with a period $T = 4F[\pi/2, (1+\psi)/2]$ when $-1 < \psi < 1$ and $T = 2[2/(1+\psi)]^{1/2} F[\pi/2, 2/(1+\psi)]$ when $1 < \psi$, where F is the incomplete elliptic integral of the first kind. The period diverges as $-\log|1-\psi|$ when the trajectory approaches the separatrix.

If all particles are initially located along the semiaxis $(x_0 = 0, y_0 > 0)$, the required time to move to the abscissa x passing once across the x axis when $-1 < \psi < 1$ is

$$t = 2F\left(\frac{\pi}{2}, \frac{1+\psi}{2}\right) - \left(\frac{2}{1+\psi}\right)^{1/2} F\left(\frac{x}{2}, \frac{2}{1+\psi}\right), \tag{A.8}$$

and the required time to move to a location x passing once across $x = \pi$ when $\psi > 1$ is

$$t = \left(\frac{2}{1+\psi}\right)^{1/2}\left[2F\left(\frac{\pi}{2}, \frac{2}{1+\psi}\right) + F\left(\frac{x}{2} - \pi, \frac{2}{1+\psi}\right)\right]. \tag{A.9}$$

Near the separatrix, taking $\psi = 1 - \epsilon$ with $\epsilon \ll 1$ and using asymptotic properties of elliptic integrals, (A.8) and (A.9) can be both simplified as

$$t = \log\left[\frac{32}{|\varepsilon|}\left|\frac{1-\tan(x/4)}{1+\tan(x/4)}\right|\right]. \tag{A.10}$$

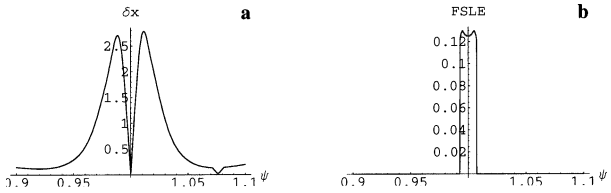

FIG. A2. (a) Separation as a function of ψ at time $t = 15$ for pairs initially located on the y axis and $\nu = 0.01$. (b) Same as (a) but for FSLE calculated for a final separation $|\delta\mathbf{x}| = 3$.

Therefore the separation of a pair $\{x_1, x_2\}$ with $\epsilon_1 = \epsilon + \nu/2$ and $\epsilon_2 = \epsilon - \nu/2$, after passing once by the hyperbolic point and if $\nu \ll \epsilon$, is

$$\delta x = -\frac{\nu}{2}\cos\frac{x}{2}, \tag{A.11}$$

where $\delta x = (x_2 - x_1)/2$ and $x = (x_2 + x_1)/2$. If the two particles are on both sides of the separatrix, with $\epsilon_1 > 0 > \epsilon_2$, the abcissas after passing once by the hyperbolic point are given by

$$-\log\left(\frac{1 + \tan\frac{1}{4}x_2}{-1 + \tan\frac{1}{4}x_2}\,\frac{1 - \tan\frac{1}{4}x_1}{1 + \tan\frac{1}{4}x_1}\right) = \log\frac{-\varepsilon_2}{\varepsilon_1}. \tag{A.12}$$

If $\epsilon_2 = -\epsilon_1$, we have $\pi - x_1 = x_2 - \pi$. After passing once by the hyperbolic point, a straddling pair is separated by a distance of $O(1)$ when the time is $O(-\log\nu)$ since there is always one particle of the pair starting at a distance to the y axis located between $\nu/2$ and ν. According to (A.11), a nonstraddling pair needs to pass $O(1/\nu)$ times by the hyperbolic point during a time of $O(-(\log\epsilon)/\nu)$ to separate over a distance of $O(1)$. Hence, for ν small enough, the separation occurs much faster for the straddling pair.

This reasoning corroborates the results found for example I but neglects the fact that the trajectories are periodic in time and, therefore, that the separations are quasiperiodic. If pairs separate by a distance $O(1)$ over a time T they meet again over a time of a few T. Owing to this saturation effect, the separation oscillates strongly within the vicinity of the separatrix introducing spurious patterns. Figure A2a shows the separation at time $t = 15$ for pairs initially aligned on the y axis. The expected maxima on $\psi = 1$ is turned into a minima and spurious maxima occur on both sides. In a more general flow with a variety of scales, portions of the hyperbolic structure are visible at a given time and then blurred out by saturation effects at later time.

The FSLE, in turn, is not sensitive to saturation effects because one calculates the shortest time required to reach a given separation. Figure A2b show the FSLE calculated using the same data as Figure A2a. The maxima is still sharply defined and surrounded by zeros for points which did not reach the required separation within the observation period.

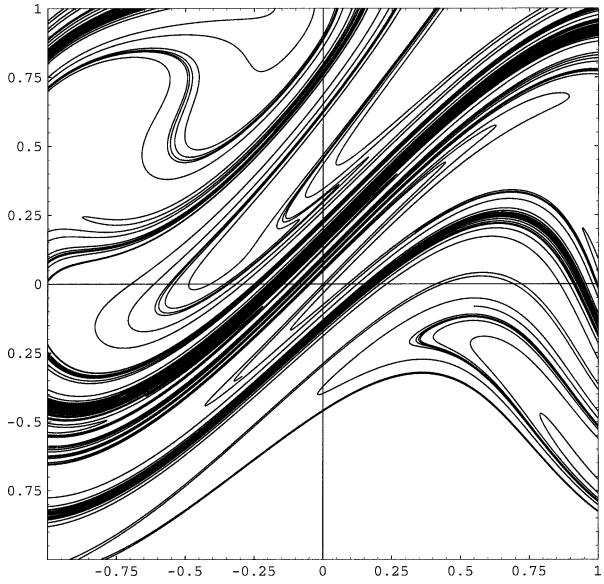

FIG. A3. The unstable manifold of the forced Duffing equation in a rotating frame plotted at time $t = 0$. See the text for the construction of this figure.

c. *Example III: The forced Duffing equation in a rotated frame*

It is undoubtly a difficult task to extend the above analytical considerations to a nonintegrable system. Our demonstration here is purely numerical. We consider the case of the forced Duffing equation in a rotating frame already used by Haller (2000). This system is given for $\mathbf{x} = (x, y)$ by

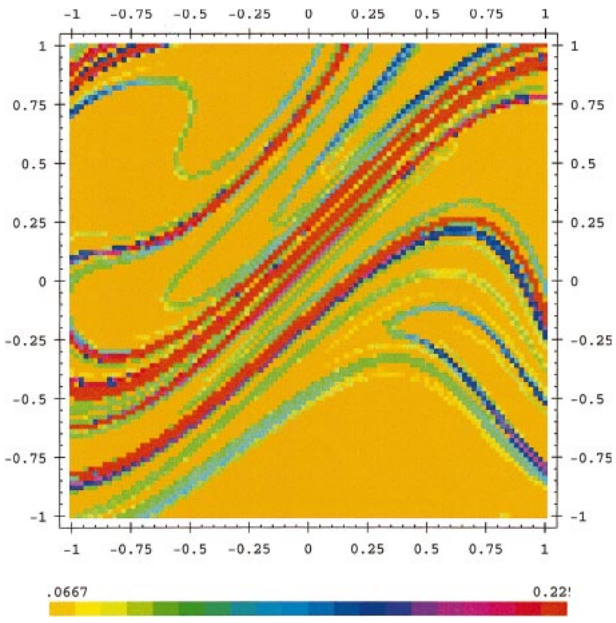

FIG. A4. The FSLE for the forced Duffing equation in a rotated frame plotted at time $t = 0$ for a separation $\delta\mathbf{x} = 1.5$ and a backward integration time $T = 15$. Values are as indicated in the caption.

$$\mathbf{x} = \mathbf{B}\mathbf{x} - \mathbf{N} + \begin{pmatrix} 0 \\ \sin\omega t \end{pmatrix}, \qquad \text{(A.13)}$$

where

$$\mathbf{B} = \begin{pmatrix} \sin 2\omega t & \omega + \cos 2\omega t \\ -\omega + \cos 2\omega t & -\sin 2\omega t \end{pmatrix} \quad \text{and}$$

$$\mathbf{N} = (x\cos\omega t - y\sin\omega t)^3 \begin{pmatrix} \sin\omega t \\ \cos\omega t \end{pmatrix}.$$

Here we take $\omega = 0.9$ and we first find the location y_c of the hyperbolic point in the Poincaré map at time $t = 0$ on the y axis by integrating forward and backward in time a small half-circle surrounding the expected hyperbolic point as in Miller et al. (1997). Using 27-digit arithmetic, we obtain $y_c = 0.170042170231512\ldots$ with 15-digit accuracy. Then we integrate for 5 periods, using 22-digit arithmetic, a set of points initially regularly spread along two small segments of length 10^{-8} along the unstable direction in order to generate the unstable manifold. At each period, the generated curve is renoded. The results have been checked by dividing the initial length of the segment by 10 and increasing the accuracy by 2 digits. Figure A3 shows the unstable manifold within the window $[-1, 1] \times [-1, 1]$. Owing to the symmetries of the problem, the stable manifold is obtained by reversing the x axis. The hyperbolic point is located where the densest bunch of lines crosses the y axis.

The FSLE algorithm is now applied on a grid of dimension 101×101 over the window $[-1, 1] \times [-1, 1]$. For a given trajectory $\mathbf{x}(\mathbf{x}_0)$ the pair separation is calculated as

$$\delta\mathbf{x} = [|\mathbf{x}(\mathbf{x}_0 + \varepsilon\mathbf{i}) - \mathbf{x}(\mathbf{x}_0 - \varepsilon\mathbf{i})|^2 + |\mathbf{x}(\mathbf{x}_0 + \varepsilon\mathbf{j}) - \mathbf{x}(\mathbf{x}_0 - \varepsilon\mathbf{j})|^2]^{1/2},$$

where $\mathbf{i}$ and $\mathbf{j}$ are the unit vectors in the x and y directions and $\epsilon = 0.01$. The pair separation is calculated for each point of the grid over a backward temporal integration of duration $T = 15$. Figure A4 shows the FSLE for a final separation $|\delta\mathbf{x}| = 1.5$. The agreement with Fig. A3 is striking. It is clear that the simple calculation of the FSLE is able to capture much of the detail of the unstable manifold.

These three examples allow us to conjecture that the maxima of FSLE map the location of the invariant hyperbolic manifolds in a large variety of flows. It would be desirable to pursue the theoretical investigations to further check this conjecture, in particular in flows with many scales of motion. We expect in this case that hyperbolic structures at various scales will be revealed by varying the distance over which the FSLE is calculated.

The study of simple diagnostic tools of the hyperbolic structure should also encompass related methods that were previously proposed like escape time plots (Rom-Kedar et al. 1990) or patchiness (Malhotra et al. 1998).

REFERENCES

Akima, H., 1991: A method of univariate interpolation that has the accuracy of a third-order polynomial. *ACM Trans. Math. Software,* **17,** 341–366.

Aref, H., 1984: Stirring by chaotic advection. *J. Fluid Mech.,* **143,** 1–21.

Artale, V., G. Boffetta, A. Celani, M. Cencini, and A. Vulpiani, 1997: Dispersion of passive tracers in closed basins: Beyond the diffusion coefficient. *Phys. Fluids,* **9,** 3162–3171.

Aurell, E., G. Boffetta, A. Crisanti, G. Paladin, and A. Vulpiani, 1997: Predictability in the large: An extension of the concept of Lyapunov exponent. *J. Phys. A: Math. Gen.,* **30,** 1–26.

Balluch, M., and P. Haynes, 1997: Quantification of lower stratospheric mixing processes using aircraft data. *J. Geophys. Res.,* **102,** 23 487–23 504.

Batchelor, G. K., 1952: The effect of homogeneous turbulence on material line surfaces. *Proc. Roy. Soc. London,* **213A,** 349–366.

Beigie, D., A. Leonard, and S. Wiggins, 1991: Chaotic transport in the homoclinic and heteroclinic tangle regions of quasi-periodically forced two-dimensional flows. *Nonlinearity,* **4,** 775–819.

——, ——, and ——, 1994: Invariant manifold templates for chaotic advection. *Chaos, Solitons, Fractals,* **4,** 749–868.

Benettin, G., D. Casati, L. Galgani, A. Giorgelli, and L. Sironi, 1986: Apparent fractal dimensions in conservative dynamical systems. *Phys. Lett.,* **118A,** 325–330.

Boffetta, G., M. Celani, G. Lacorata, and A. Vulpiani, 2000: Nonasymptotic properties of transport and mixing. *Chaos,* **10,** 50–60.

Bowman, K. P., 1993: Large-scale isentropic mixing properties of the Antarctic polar vortex from analyzed winds. *J. Geophys. Res.,* **98,** 23 013–23 027.

Chen, S., and R. Kraichnan, 1998: Simulation of a randomly advected passive scalar field. *Phys. Fluids,* **10,** 2867–2884.

Coppel, W., 1978: *Dichotomies in Stability Theory.* Lecture Notes in Mathematics, Vol. 629, Springer-Verlag, 97 pp.

Couliette, C., and S. Wiggins, 2000: Intergyre transport in a wind-driven, quasi-geostrophic double gyre: An application of lobe dynamics. *Nonlinear Proc. Geophys.,* **7,** 59–85.

Dahlberg, S. P., and K. P. Bowman, 1994: Climatology of large-scale isentropic mixing in the Arctic winter stratosphere from analysed winds. *J. Geophys. Res.,* **99,** 20 585–20 599.

del Castillo-Negrete, D., 1998: Asymmetric transport and non-Gaussian statistics of passive scalars in vortices in shear. *Phys. Fluids,* **5,** 576–594.

Drazin, P. G., 1992: *Nonlinear Systems.* Cambridge Texts in Applied Mathematics, No. 10, Cambridge University Press, 320 pp.

Dritschel, D., 1989: Contour dynamics and contour surgery: Numerical algorithms for extended, high-resolution modelling of vortex dynamics in two-dimensional, inviscid, incompressible flows. *Comput. Phys. Rep.,* **10,** 77–146.

Duan, J., and S. Wiggins, 1996: Fluid exchange across a meandering jet with a quasi-periodic variability. *J. Phys. Oceanogr.,* **26,** 1176–1188.

Eckart, C., 1948: An analysis of stirring and mixing processes in incompressible fluids. *J. Mar. Res.,* **7,** 265–275.

Frisch, U., A. Mazzino, and M. Vergassola, 1998: Intermittency in passive scalar advection. *Phys. Rev. Lett.,* **80,** 5532–5535.

Haller, G., 2000: Finding finite-time invariant manifolds in two-dimensional velocity fields. *Chaos,* **10,** 99–108.

——, 2001: Lagrangian coherent structures and the rate of strain in two-dimensional turbulence. *Phys. Fluids,* **13,** 3365–3385.

——, and A. Poje, 1998: Finite time transport in aperiodic flows. *Physica D,* **119,** 352–380.

——, and G. Yuan, 2000: Lagrangian coherent structures and mixing in two-dimensional turbulence. *Physica D,* **147,** 352–370.

Haynes, P., and E. Shuckburgh, 2000: Effective diffusivity as a diagnostic of atmospheric transport. Part I: Stratosphere. *J. Geophys. Res.,* **105,** 22 777–22 794.

Hénon, M., 1966: Sur la topologie des lignes de courant dans un cas particulier. *C. R. Acad. Sci. Paris,* **262,** 312–314.

Holton, J. R., P. H. Haynes, M. E. McIntyre, A. R. Douglass, R. B. Rood, and L. Pfister, 1995: Stratosphere–troposphere exchange. *Rev. Geophys.,* **33,** 430–439.

Juckes, M., and M. E. McIntyre, 1987: A high resolution, one-layer model of breaking planetary waves in the stratosphere. *Nature,* **328,** 590–596.

Koh, T.-Y., and R. Plumb, 2000: Lobe dynamics applied to barotropic Rossby-wave breaking. *Phys. Fluids,* **12,** 1518–1528.

Kraichnan, R. H., 1994: Anomalous scaling of randomly advected passive scalar. *Phys. Rev. Lett.,* **72,** 1016–1019.

Lacorata, G., E. Aurell, and A. Vulpiani, 2001: Relative dispersion in the Adriatic Sea: Lagrangian data and chaotic model. *Ann. Geophys.* **19,** 1–9.

Lawden, D. F., 1989: *Elliptic Functions and Applications.* Applied Mathematical Sciences, Vol. 80, Springer-Verlag, 334 pp.

Mackay, R., J. Meiss, and I. Percival, 1984: Transport in Hamiltonian systems. *Physica D,* **13,** 55–81.

Malhotra, N., and S. Wiggins, 1999: Geometric structures, lobe dynamics, and Lagrangian transport in flows with aperiodic time-dependence, with applications to Rossby wave flow. *J. Nonlinear Sci.,* **8,** 401–456.

——, I. Mezíc, and S. Wiggins, 1998: Patchiness: A new diagnostic for Lagrangian trajectory analysis in time-dependent fluid flows. *Int. J. Bifurcation Chaos,* **8,** 1053–1093.

Mariotti, A., M. Moustaoui, B. Legras, and H. Teitelbaum, 1997: Comparison between vertical ozone soundings and reconstructed potential vorticity maps by contour advection with surgery. *J. Geophys. Res.,* **102,** 6131–6142.

——, C. Mechoso, B. Legras, and Y. Chi, 2000: The evolution of the ozone ''collar'' in the Antarctic lower stratosphere during early August 1994. *J. Atmos. Sci.,* **57,** 402–414.

McAllister, D., and J. Roulier, 1981: An algorithm for computing a shape-preserving oscillatory quadratic spline. *ACM Trans. Math. Software,* **7,** 331–347.

McIntyre, M., 1995: The stratospheric polar vortex and sub-vortex: Fluid dynamics and midlatitude ozone loss. *Philos. Trans. Roy. Meteor. Soc.,* **352A,** 227–240.

——, and T. Palmer, 1984: The surf zone in the stratosphere. *J. Atmos. Sci. Terr. Phys.,* **46,** 825–849.

Miller, P., C. Jones, A. Rogerson, and L. Pratt, 1997: Quantifying transport in numerically generated velocity fields. *Physica D,* **110,** 105–122.

Nakamura, N., 1996: Two-dimensional mixing, edge formation, and permeability diagnosed in an area coordinate. *J. Atmos. Sci.,* **53,** 1524–1537.

Ngan, K., and T. G. Shepherd, 1999: A closer look at chaotic advection in the stratosphere. Part I: Geometric structure. *J. Atmos. Sci.,* **56,** 4134–4152.

Ottino, J. M., 1989: *The Kinematics of Mixing: Stretching, Chaos and Transport.* Cambridge University Press, 364 pp.

Pierce, R. B., and T. D. Fairlie, 1993: Chaotic advection in the stratosphere: Implications for the dispersal of chemically perturbed air from the polar vortex. *J. Geophys. Res.,* **98D,** 18 589–18 595.

——, ——, W. Grose, R. Swinbank, and A. O'Neill, 1994: Mixing processes within the polar night jet. *J. Atmos. Sci.,* **51,** 2957–2972.

Pierrehumbert, R., 1991a: Large-scale horizontal mixing in planetary atmospheres. *Phys. Fluids,* **3,** 1250–1260.

——, 1991b: Chaotic mixing of tracers and vorticity by modulated travelling Rossby wave. *Geophys. Astrophys. Fluid Dyn.,* **58,** 285–320.

——, and H. Yang, 1993: Global chaotic mixing on isentropic surfaces. *J. Atmos. Sci.,* **50,** 2462–2480.

Plumb, R., and Coauthors, 1994: Intrusions into the lower stratospheric Arctic vortex during the winter of 1991/92. *J. Geophys. Res.,* **99,** 1089–1105.

——, D. W. Waugh, and M. P. Chipperfield, 2000: The effects of mixing on tracer relationships in the polar vortex. *J. Geophys. Res.,* **105,** 10 047–10 062.

Rhines, P. B., and W. R. Young, 1983: How rapidly is a passive scalar mixed within closed streamlines? *J. Fluid Mech.,* **133,** 133–145.

Richardson, L., 1926: Atmospheric diffusion shown on a distance-neighbour graph. *Philos. Trans. Roy. Soc. London,* **110A,** 709–737.

Rom-Kedar, V., A. Leonard, and S. Wiggins, 1990: An analytical study of transport, mixing and chaos in an unsteady vortical flow. *J. Fluid Mech.,* **214,** 347–394.

Sobel, A., and R. Plumb, 1999: Quantitative diagnostics of mixing in a shallow water model of the stratosphere. *J. Atmos. Sci.,* **56,** 2811–2829.

Tuck, A., 1989: Synoptic and chemical evolution of the Antarctic vortex in late winter and early spring. *J. Geophys. Res.,* **94,** 11 687–11 737.

Waugh, D., and Coauthors, 1994: Transport out of the lower stratospheric Arctic vortex by Rossby wave breaking. *J. Geophys. Res.,* **99,** 1071–1088.

——, and Coauthors, 1997: Mixing of polar air into middle latitudes as revealed by tracer–tracer scatter plots. *J. Geophys. Res.,* **102,** 13 119–13 134.

WMO, 1999: Scientific assessment of ozone depletion: 1998. Global Ozone Research and Monitoring Project Rep. 44, World Meteorological Organization, Geneva, Switzerland, 605 pp.

Zaslavsky, G. M., 1998: *Physics of Chaos in Hamiltonian Systems.* Imperial College Press, 269 pp.